CORONAVIRUS

PD-1/PD-L1 blockade abrogates a dysfunctional innate-adaptive immune axis in critical β-coronavirus disease

Maite Duhalde Vega[1]†‡, Daniela Olivera[1,2]†, Gustavo Gastão Davanzo[3]†, Mauricio Bertullo[4], Verónica Noya[5], Gabriela Fabiano de Souza[6], Stéfanie Primon Muraro[6], Icaro Castro[7], Ana Paula Arévalo[8], Martina Crispo[8], Germán Galliussi[9], Sofía Russo[1,2], David Charbonnier[1], Florencia Rammauro[2,10], Mathías Jeldres[1,2], Catalina Alamón[11], Valentina Varela[11], Carlos Batthyany[9], Mariela Bollati-Fogolín[12], Pablo Oppezzo[13], Otto Pritsch[2,10], José Luiz Proença-Módena[6], Helder I. Nakaya[7], Emiliano Trias[11], Luis Barbeito[11], Ignacio Anegon[14], María Cristina Cuturi[14]§, Pedro Moraes-Vieira[3]§, Mercedes Segovia[1,2]*§, Marcelo Hill[1,2]*§

Severe COVID-19 is associated with hyperinflammation and weak T cell responses against SARS-CoV-2. However, the links between those processes remain partially characterized. Moreover, whether and how therapeutically manipulating T cells may benefit patients are unknown. Our genetic and pharmacological evidence demonstrates that the ion channel TMEM176B inhibited inflammasome activation triggered by SARS-CoV-2 and SARS-CoV-2–related murine β-coronavirus. *Tmem176b*$^{-/-}$ mice infected with murine β-coronavirus developed inflammasome-dependent T cell dysfunction and critical disease, which was controlled by modulating dysfunctional T cells with PD-1 blockers. In critical COVID-19, inflammasome activation correlated with dysfunctional T cells and low monocytic TMEM176B expression, whereas PD-L1 blockade rescued T cell functionality. Here, we mechanistically link T cell dysfunction and inflammation, supporting a cancer immunotherapy to reinforce T cell immunity in critical β-coronavirus disease.

INTRODUCTION

Coordinated innate and adaptive immunity triggered by pathogenic human and animal β-coronaviruses are thought to prevent severe disease through conserved mechanisms (*1–6*). Accordingly, when severe coronavirus disease 2019 (COVID-19) arises, it is associated with dysregulated innate immunity (hyperinflammation), weak T cell responses, and high viral load (*3, 5, 7–10*). Thus, dysfunctional innate and adaptive immune responses may lead to uncontrolled viral replication and life-threatening disease. Nevertheless, whether hyperinflammation affects T cell immunity needs further research. Monoclonal antibodies blocking the proinflammatory interleukin-6 (IL-6) receptor may add some therapeutic benefit in COVID-19 patients, although seemingly contradictory results have been reported (*11–13*). However, this therapy does not necessarily control viral load (*14*). CD8$^+$ T cell responses have the potential capacity to control viral replication by killing infected cells (*15*). Nevertheless, therapeutic strategies aiming to reinforce T cell responses in β-coronavirus disease have not been developed. This scenario may be explained because (i) it is still unclear whether impaired T cell immunity causes severe disease (*9*) and (ii) the mechanisms leading to low T cell responses remain only partially understood (*16, 17*). Thus, characterizing these issues may help to repurpose and/or develop rational immunotherapies targeting T cells in critical COVID-19 patients.

T cells appear to be dysfunctional in COVID-19, although contradictory data have been published in this field (*8, 18–23*). Exhausted T cells are a specific lineage of dysfunctional cells characterized by impaired effector mechanisms and transcriptional, epigenetic, and metabolic programs as well as the expression of inhibitory receptors such as programmed cell death 1 (PD-1) (*24, 25*). Therapeutically, T cell exhaustion can be modulated by blocking PD-1 and its cognate ligand PD-L1 (*26*). PD-1/PD-L1 blockade improves disease-free and overall survival in several human cancers (*27*). However, it remains unknown whether PD-1/PD-L1 blockade may benefit COVID-19 patients (*28*). A mechanistic understanding of T cell dysfunction in β-coronavirus disease is necessary to validate and rationalize this approach. The efficacy of PD-1/PD-L1 blockers may be determined, at least in part, by the inflammatory context (*29*). Thus, characterizing potential links between inflammation and T cell dysfunction may help to select COVID-19 patients who could benefit from PD-1/PD-L1 blockade. We have proposed that

[1]Laboratory of Immunoregulation and Inflammation, Institut Pasteur de Montevideo, 11400 Montevideo, Uruguay. [2]Immunobiology Department, Faculty of Medicine, University of the Republic, 11800 Montevideo, Uruguay. [3]Laboratory of Immunometabolism, Department of Genetics, Evolution, Microbiology and Immunology, Institute of Biology, University of Campinas, SP, Brazil. [4]Intensive Care Unit, CASMU, 11600 Montevideo, Uruguay. [5]Laboratory of Molecular Biology, Sanatorio Americano, 11600 Montevideo, Uruguay. [6]Laboratory of Emerging Viruses, Department of Genetics, Evolution, Microbiology and Immunology, Institute of Biology, University of Campinas, SP, Brazil. [7]Hospital Israelita Albert Einstein, SP, Brazil. [8]Laboratory Animals Biotechnology, Institut Pasteur de Montevideo, 11400 Montevideo, Uruguay. [9]Laboratory of Vascular Biology and Drug Development, Institut Pasteur de Montevideo, 11400 Montevideo, Uruguay. [10]Laboratory of Immunovirology, Institut Pasteur de Montevideo, 11400 Montevideo, Uruguay. [11]Laboratorio de Neurodegeneración, Institut Pasteur de Montevideo, 11400 Montevideo, Uruguay. [12]Cell Biology Unit, Institut Pasteur de Montevideo, 11400 Montevideo, Uruguay. [13]Research Laboratory on Chronic Lymphocytic Leukemia, Institut Pasteur de Montevideo, 11400 Montevideo, Uruguay. [14]INSERM UMR 1064, Center for Research in Transplantation and Immunology; Université de Nantes; CHU Nantes, Institut de Transplantation Urologie Néphrologie (ITUN), 44093 Nantes, France.
*Corresponding author. Email: msegovia@pasteur.edu.uy (M.S.); mhill@pasteur.edu.uy (M.H.)
†These authors contributed equally to this work.
‡Present address: Institute of Biological Chemistry and Chemical Physics (UBA-CONICET), Faculty of Pharmacy and Biochemistry, University of Buenos Aires, Junín 956 (C1113AAD), Buenos Aires, Argentina.
§These authors contributed equally to this work as co–senior authors.

T cell exhaustion may be controlled by inflammasomes in cancer (*29*). Inflammasomes are cytosolic multiprotein complexes that sense cellular stress. Once activated, they cleave caspase-1, which then processes pro–IL-1β and pro–IL-18, among other substrates, to yield the active and secreted forms of these cytokines (*30*). In myeloid cells, NLRP3 inflammasomes are inhibited through ionic mechanisms by the CD20-like MS4A family member TMEM176B, an intracellular acid–sensitive nonspecific cation channel (*29, 31–34*). Furthermore, *TMEM176B* was found to be overexpressed in monocytes from nonpneumonia versus its expression in those from pneumonia COVID-19 patients (*35*). We therefore speculated that TMEM176B-regulated inflammasomes may trigger T cell dysfunction in β-coronavirus infection.

Here, we show that TMEM176B controls inflammasome activation triggered by severe acute respiratory syndrome coronavirus 2 (SARS-CoV-2) and SARS-CoV-2–related murine hepatitis virus (MHV)–A59. Moreover, unleashed inflammasome activation leads to T cell dysfunction in the context of β-coronavirus infection. Last, PD-1/PD-L1 blockade restores T cell functionality in vitro in critical COVID-19 patients and in vivo in MHV-A59–infected $Tmem176b^{-/-}$ mice.

RESULTS

TMEM176B is a protective host factor in β-coronavirus infection by controlling inflammasome activation

We first analyzed published single-cell RNA sequencing data from bronchioalveolar lavage (BAL) samples from moderately and severely ill patients (*36*). The expression of *TMEM176B* and the homologous gene *TMEM176A* was significantly down-regulated in BAL macrophages from severely ill patients versus in those from moderately ill patients (Fig. 1A). In contrast, *IL1B*, *NLRP3*, and *IL1R2* were up-regulated in BAL macrophages from severely ill patients (Fig. 1A). Next, we determined TMEM176B protein expression in CD14$^+$ monocytes of peripheral blood from healthy donors (HDs), non–intensive care unit (non-ICU) patients, and ICU patients (fig. S1 and table S1). TMEM176B expression was inversely correlated with plasma active caspase-1 levels in the ICU patients but not in the non-ICU patients (Fig. 1B). Because TMEM176B controls inflammasome activation through ionic mechanisms (*31*), we then assessed whether TMEM176B may control inflammasome activation triggered by the SARS-CoV-2 ion channel envelope (E) protein. Transfection of THP-1 cells with SARS-CoV-2 E protein triggered IL-1β secretion (Fig. 1C) and caspase-1 activation (fig. S2A), which were inhibited by cotransfecting cells with *TMEM176B* (Fig. 1, D and E) without affecting cell viability (fig. S2B). Thus, data from patients and genetic in vitro experiments support a role for TMEM176B in controlling SARS-CoV-2–induced inflammasome activation.

To further study a potential role for TMEM176B as a host-protective factor in β-coronavirus disease, we then worked with MHV-A59. MHV-A59 is a widely used β-coronavirus model that has been shown to induce conserved innate and adaptive immune responses in relationship to SARS-CoV-2 (*1–6, 37*). Moreover, liver injury is a frequent extrapulmonary manifestation of critically ill COVID-19 patients (*38*). We first observed that MHV-A59 peaked at 5 days post-infection (dpi) in the liver of wild-type (WT) mice (fig. S3A). *Tmem176b* expression was induced by MHV-A59 in the liver of WT mice peaking at 3 dpi (fig. S3B). Moreover, in infected animals, Tmem176b colocalized with major histocompatibility complex

(MHC) II staining, suggesting its expression by dendritic cells (DCs) in the liver (fig. S3C). The analysis of the survival rates revealed that $Tmem176b^{-/-}$ mice were highly susceptible to MHV-A59, in clear contrast to WT animals that controlled the infection (Fig. 1F). Compared to WT animals, $Tmem176b^{-/-}$ mice also showed increased levels of MHV RNA in the liver (Fig. 1G) and plasma glutamic-pyruvic transaminase (GPT) activity (Fig. 1H). Inflammasome activation has been shown to be associated with a worse outcome in MHV-infected mice (*39*). Thus, *Tmem176b* may protect the host by inhibiting MHV-induced inflammasome activation. Accordingly, we found that the livers of infected $Tmem176b^{-/-}$ mice showed higher levels of active IL-1β (17 kDa) and caspase-1 (20 kDa) than those of WT animals (Fig. 1, I and J). Flow cytometry analysis showed enhanced caspase-1 activation in CD11b$^-$ and CD11b$^+$ conventional DCs from $Tmem176b^{-/-}$ mice compared to those from WT animals (Fig. 1, K and L, and fig. S4). Moreover, *Tmem176b* controlled the ability of MHV-A59 to activate NLRP3 inflammasomes in bone marrow–derived DCs (BMDCs) in vitro (fig. S5). Thus, *Tmem176b* regulates inflammasome activation in DCs induced by MHV-A59 infection in vitro and in vivo. We then wished to directly demonstrate a role for enhanced inflammasome activation in the worse outcome of $Tmem176b^{-/-}$ mice. IL-1β blockade (Fig. 1M) and *Casp1* deletion (Fig. 1N) significantly diminished the viral load and improved mouse survival in $Tmem176b^{-/-}$ animals (Fig. 1O). Furthermore, inflammasome activation in $Tmem176b^{-/-}$ mice may lead to impaired immunity against MHV-A59. Accordingly, depletion of CD8$^+$ T cells abolished the improvement in survival and viral load control obtained with anti–IL-1β antibody treatment (Fig. 1, M and O, and fig. S6). These results suggest that unleashed inflammasome activation in $Tmem176b^{-/-}$ DCs impairs MHV control, likely by regulating CD8$^+$ T cells.

Inflammasome-dependent CD8$^+$ T cell exhaustion in $Tmem176b^{-/-}$ mice infected with MHV-A59

To further support a pathogenic mechanism involving DCs and CD8$^+$ T cells in MHV-A59–infected $Tmem176b^{-/-}$ mice, we performed adoptive cell transfer (ACT) experiments. We observed that ACT of $Tmem176b^{-/-}$ splenic DCs from infected mice into WT recipients infected with MHV-A59 decreased survival (Fig. 2A). Moreover, ACT of CD8$^+$ T cells from infected WT animals rescued the survival of infected $Tmem176b^{-/-}$ mice (Fig. 2A). Thus, enhanced inflammasome activation in DCs impairs anti–MHV-A59 immunity mediated by CD8$^+$ T cells. Accordingly, $Tmem176b^{-/-}$ mice had lower MHV-specific in vivo CD8-dependent cytotoxicity than WT and $Tmem176b^{-/-}Casp1^{-/-}$ animals (Fig. 2, B and C). In agreement with a detrimental role of inflammasome activation in CD8$^+$ T cell responses against MHV-A59, $Casp1/11^{-/-}$ mice showed reinforced anti–MHV-A59 CD8$^+$ T cell responses versus those in C57BL/6JN WT controls (fig. S7).

We then aimed to characterize the mechanisms by which CD8$^+$ T cell responses were modulated by inflammasomes in MHV-A59 infection. We analyzed exhausted CD8$^+$ T lymphocytes within MHV-A59–specific cells in infected animals. We observed increased progenitor exhausted MHV-specific CD8$^+$ T cells (CD44$^+$ PD-1$^+$ TCF-1$^+$ TOX$^+$) in $Tmem176b^{-/-}$, compared to WT mice, but not in $Tmem176b^{-/-}Casp1^{-/-}$ animals (Fig. 2, D and E). *Casp1* deletion in $Tmem176b^{-/-}$ animals rescues the survival, viral load, in vivo CD8-dependent cytotoxicity, and relative number of exhausted CD8$^+$ T cells, demonstrating a role for inflammasomes in the enhanced
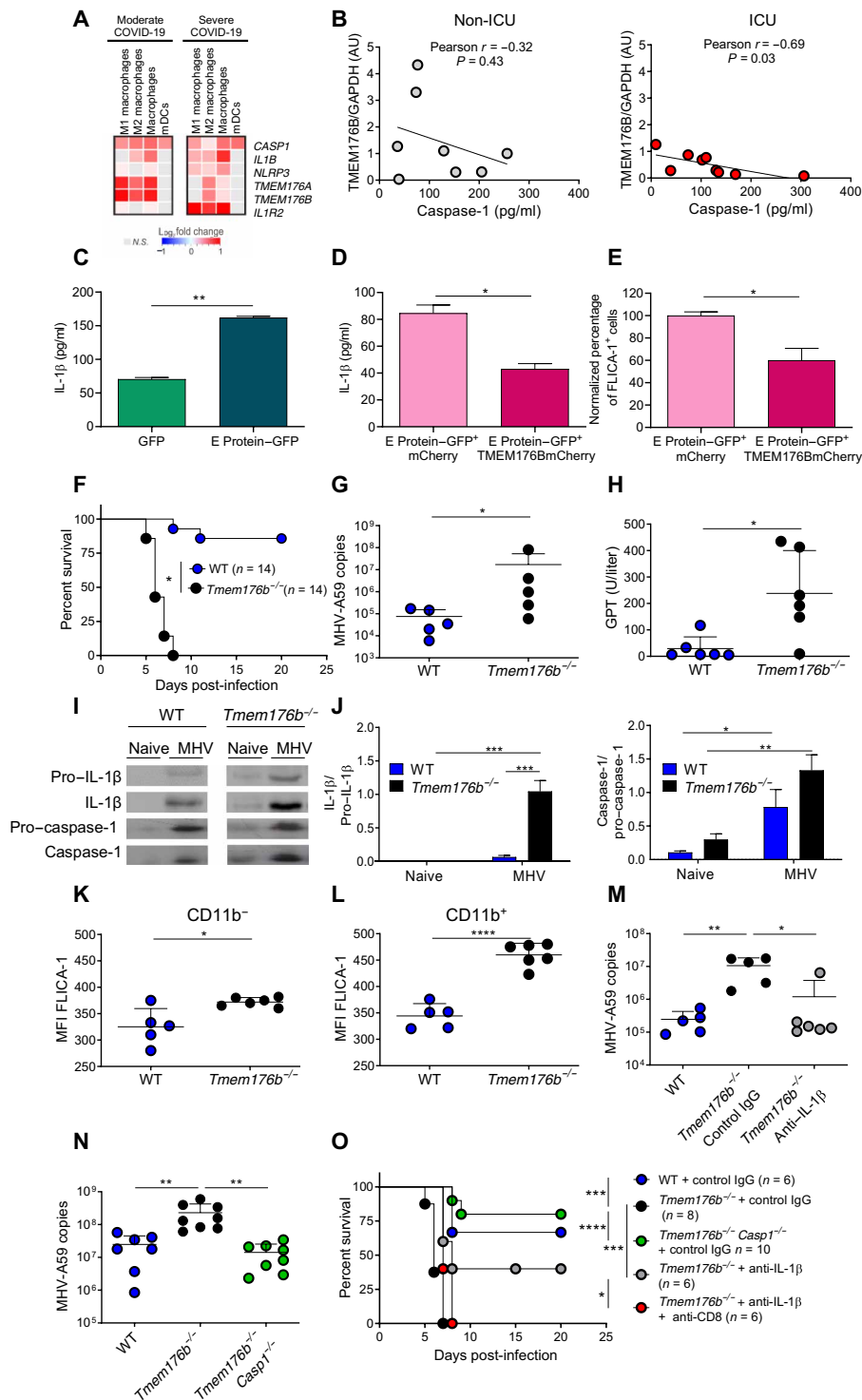
Fig. 1. TMEM176B is a protective host factor in β-coronavirus infection by controlling inflammasome activation. (**A**) Heatmaps of indicated transcripts. Analysis of published data (*36*). (**B**) Correlation study of TMEM176B/glyceraldehyde-3-phosphate dehydrogenase (GAPDH) ratio in CD14+ cells with plasmatic active caspase-1. AU, arbitrary units. (**C**) E protein triggers IL-1β secretion by THP-1 monocytes. One experiment representative of three is shown. **$P < 0.01$, Student's *t* test. (**D** and **E**) IL-1β secretion and active caspase-1 triggered by E protein were inhibited by TMEM176B in THP-1 monocytes. One experiment representative of three is shown in (D), and a pool of two experiments is shown in (E). *$P < 0.05$, Student's *t* test. (**F**) Survival of MHV-A59–infected mice. *$P < 0.05$, log-rank (Mantel-Cox) test. (**G**) Viral load in the liver at 5 days post-infection (dpi). *$P < 0.05$, Student's *t* test. (**H**) Serum plasma glutamic-pyruvic transaminase (GPT) transaminase activity at 5 dpi. *$P < 0.05$, Student's *t* test. (**I**) Western blot study in the liver at 5 dpi. (**J**) Semiquantification of Western blot bands. *$P < 0.05$; **$P < 0.01$; ***$P < 0.001$, two-way analysis of variance (ANOVA) test. (**K** and **L**) Percentage of FLICA-1+ cells within CD11c+ MHC II+ CD11b− and CD11b+ cells. *$P < 0.05$; ****$P < 0.0001$, Student's *t* test. (**M** and **N**) Viral load in the liver at 5 dpi. *$P < 0.05$; **$P < 0.01$, one-way ANOVA test. (**O**) Survival in infected mice. *$P < 0.05$; ***$P < 0.001$; ****$P < 0.0001$, log-rank (Mantel-Cox) test.
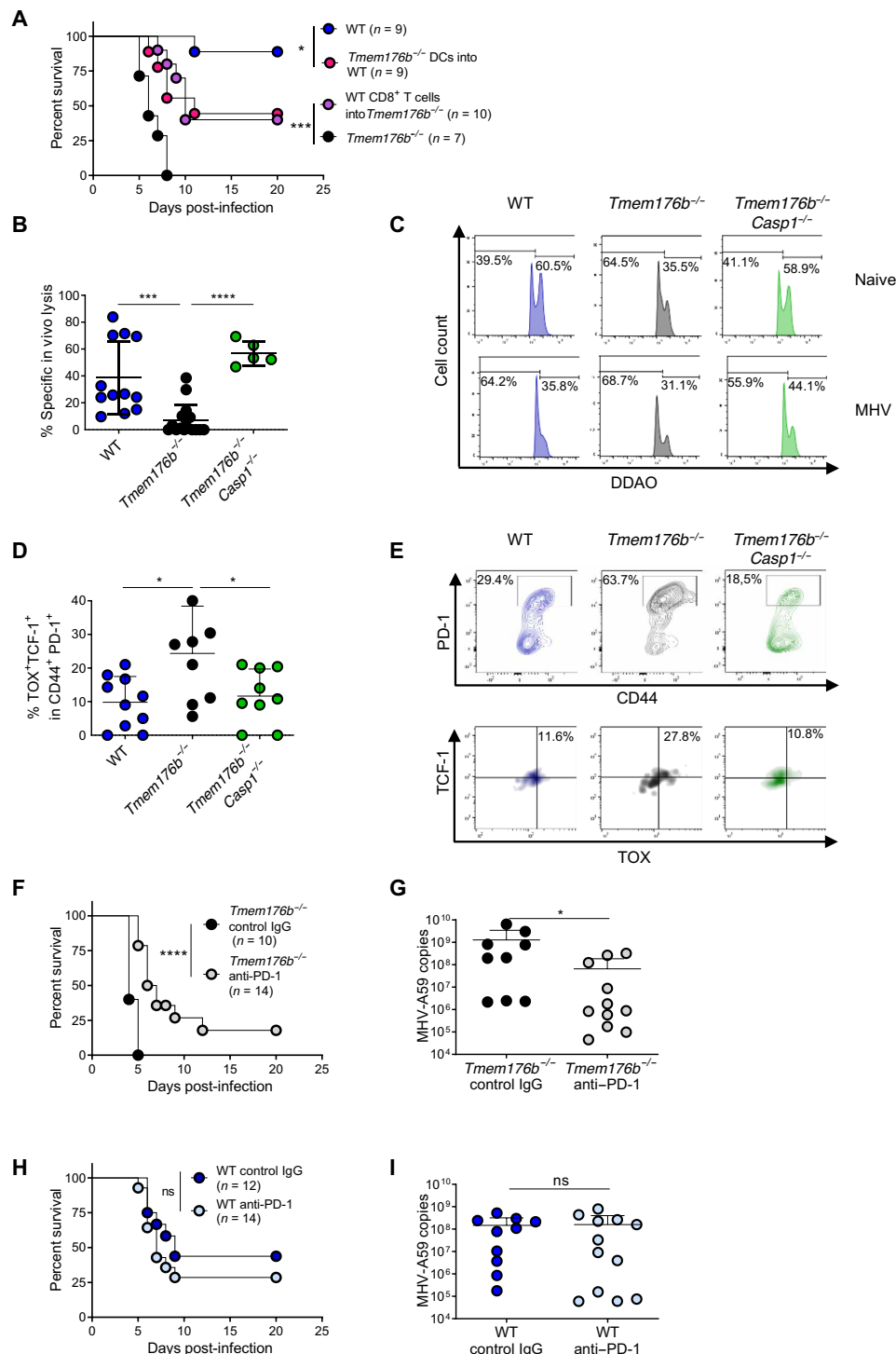
Fig. 2. Inflammasome-dependent T cell exhaustion in *Tmem176b*^{−/−} mice infected with MHV-A59. (**A**) Survival of MHV-A59–infected WT and *Tmem176b*^{−/−} mice left untreated. In another group, infected WT mice were adoptively transferred with splenic DCs from infected *Tmem176b*^{−/−} animals, and *Tmem176b*^{−/−} mice were adoptively transferred with CD8^{+} T cells from infected WT animals. *$P < 0.05$; ***$P < 0.001$, log-rank (Mantel-Cox) test. (**B**) Percentage of MHV-A59–specific CD8-dependent in vivo lysis was calculated with the formula described in Materials and Methods. Twelve WT, 16 *Tmem176b*^{−/−}, and 5 *Tmem176b*^{−/−}*Casp1*^{−/−} mice were studied at 5 dpi. ***$P < 0.001$; ****$P < 0.0001$, one-way ANOVA test. (**C**) Representative histograms of the experiments shown in (B). (**D**) Percentage of liver-infiltrating TOX^{+} TCF-1^{+} within PD-1^{+} CD44^{+} cells, gated in CD8^{+} MHV-A59–specific T cells. Animals from two independent experiments were analyzed. *$P < 0.05$, one-way ANOVA test. (**E**) Representative dot plots of the animals analyzed in (D). (**F**) Survival of *Tmem176b*^{−/−} mice infected with MHV-A59 and treated with control IgG or anti–PD-1 antibody. ****$P < 0.0001$, log-rank (Mantel-Cox) test. (**G**) Viral load in the liver at 5 dpi with MHV-A59 in *Tmem176b*^{−/−} mice treated with control IgG or anti–PD-1 antibodies. *$P < 0.05$, Mann-Whitney test. (**H**) Survival of WT mice infected with MHV-A59 and treated with control IgG or anti–PD-1 antibody. ns, nonsignificant. Log-rank (Mantel-Cox) test. (**I**) Viral load in the liver at 5 dpi with MHV-A59 in WT mice treated with control IgG or anti–PD-1 antibodies. Mann-Whitney test.

susceptibility of $Tmem176b^{-/-}$ mice to MHV-A59 infection and restricted CD8$^+$ T cell responses in those animals. Our observations thus support a role for inflammasome-dependent T cell exhaustion as a pathogenic mechanism in $Tmem176b^{-/-}$ mice. T cell exhaustion was first shown to be partially reversed by PD-1 blockade during chronic viral infection (26). We then studied whether PD-1 blockade could improve the outcome of $Tmem176b^{-/-}$ mice infected with murine β-coronavirus. Anti–PD-1 antibodies improved the survival and viral load of $Tmem176b^{-/-}$ animals upon MHV-A59 infection (Fig. 2, F and G) but lacked efficacy against mild/moderate disease in WT animals (Fig. 2, H and I). Thus, our results show that the inflammasome-exhausted T cell axis regulated by TMEM176B is a key mechanism in determining biological responses to PD-1/PD-L1 blockade.

Pharmacological modulation of the inflammasome/dysfunctional T cell axis triggered by SARS-CoV-2 in vitro

Having provided genetic evidence that TMEM176B controls inflammasome activation triggered by SARS-CoV-2 and MHV-A59 and that this cation channel plays a host-protective role by limiting the inflammasome/dysfunctional T cell axis, we then wished to pharmacologically modulate this pathway. We hypothesized that triggering TMEM176B activity in human monocytes would block SARS-CoV-2–induced inflammasome activation and T cell dysfunction. We found that the flavonoid isoquercitin (ISQ) triggers TMEM176B-dependent ion transport (Fig. 3A). ISQ treatment inhibited SARS-CoV-2–induced IL-1β secretion (Fig. 3B) without affecting viral load (Fig. 3C). ISQ also inhibited caspase-1 activation (Fig. 3, D and E), showing that this flavonoid inhibits SARS-CoV-2–induced inflammasome activation in human CD14$^+$ monocytes. Accordingly, the related compound quercetin was recently shown to control liver infection by MHV-A59 in mice (1). Moreover, quercetin therapy resulted in clinical improvement in two COVID-19 clinical trials (NCT04578158 and NCT04861298) (40, 41). We then assessed whether conditioned culture medium (CCM) from SARS-CoV-2–infected human primary monocytes could modulate alloreactive T cells. We observed that compared to CCM from uninfected (Mock) monocytes, CCM from infected monocytes induced PD-1 expression by CD8$^+$ (Fig. 3F) and CD4$^+$ (fig. S8) T cells. ISQ treatment of infected monocytes impaired SARS-CoV-2–induced CD8$^+$ (Fig. 3F) and CD4$^+$ (fig. S8) PD-1 expression. Moreover, PD-1 blockade significantly increased interferon-γ (IFN-γ) production by CD8$^+$ (Fig. 3, G and H) and CD4$^+$ (fig. S8) T cells in the presence of CCM from infected monocytes but not in the presence of CCM from uninfected cells. Thus, pharmacological activation of TMEM176B and PD-1/PD-L1 blocker treatment can abrogate T cell modulation induced by soluble factors produced by SARS-CoV-2–infected monocytes. We previously showed that blockade of IL-1β controls T cell modulation by the CCM of SARS-CoV-2–infected monocytes (18). Thus, our results suggest that T cell dysfunction driven by TMEM176B-unleashed inflammasomes is triggered by SARS-CoV-2 in human monocytes.

The inflammasome/dysfunctional T cell axis is associated with severity of COVID-19

We then studied whether inflammasome activation may correlate with exhausted T cells in critical COVID-19. PD-1 expression and T cell exhaustion are thought to be driven by high levels of the transcriptional regulator thymocyte selection-associated high mobility group box (TOX), whereas the functional role of low TOX levels in nonexhausted human T cells remains unknown (42–45). We first studied CD8$^+$ T cell activation (CD38$^+$ HLA-DR$^+$) in HDs and in ICU versus non-ICU COVID-19 patients (figs. S9 and S10). We then analyzed PD-1 and TOX expression within the activated CD8$^+$ T cells. ICU patients showed an increase in PD-1$^+$ TOX$^+$ cell percentages compared to those in non-ICU patients (Fig. 4, A and B) and HDs (fig. S9). We also observed a strong correlation between TOX and genes coding for inhibitory receptors in peripheral blood from severely ill COVID-19 patients but not from moderately ill COVID-19 patients from a previously published cohort (Fig. 4C and fig. S11) (46). In our cohort, we observed a significant positive correlation between the mean fluorescence intensity (MFI) for TOX and PD-1 within CD38$^+$ HLA-DR$^+$ CD8$^+$ T cells in the ICU patients but not in the non-ICU patients (Fig. 4D), suggesting that PD-1 is under the control of TOX in ICU patients. Thus, TOX$^+$ CD8$^+$ T cells may be exhausted in critically ill patients. We then found that exhaustion and inflammasome-related gene expression were highly correlated in severely ill patients but not in moderately ill patients from the McClain cohort (Fig. 4E and fig. S12) (46). Moreover, relative frequencies of PD-1$^+$ TOX$^+$ cells in CD38$^+$ HLA-DR$^+$ CD8$^+$ T lymphocytes positively correlated with plasma active caspase-1 levels in the ICU but not in the non-ICU patients (Fig. 4F). However, other inflammatory parameters did not correlate with the percentages of those cells in ICU patients (fig. S13). Thus, exhausted CD8$^+$ T cells may be specifically controlled by inflammasomes in critically ill patients. In noncritically ill patients, the percentage of PD-1$^+$ TOX$^+$ cells within CD38$^+$ HLA-DR$^+$ CD8$^+$ T lymphocytes might be regulated by inflammasome-independent mechanisms (Fig. 4F and fig. S13). Active plasma caspase-1 levels, PD-1$^+$ TOX$^+$ CD8$^+$ T cell levels, and TMEM176B expression by CD14$^+$ monocytes were all not associated with humoral immune responses in ICU patients (fig. S14) or comorbidities (fig. S15). We then assessed whether in vitro PD-L1 blockade may abrogate T cell dysfunction in critically ill patients. Treatment of peripheral blood mononuclear cells (PBMCs) from ICU COVID-19 patients with SARS-CoV-2 peptides was associated with increased percentages of PD-1$^+$ TOX$^+$ cells (Fig. 4G) but failed to significantly trigger IFN-γ production (Fig. 4H). In contrast, PD-L1 blockade rescued IFN-γ production in antigenic peptide-treated cells (Fig. 4H) but did not modify the percentage of PD-1$^+$ TOX$^+$ cells (Fig. 4G). Similar results were observed when tumor necrosis factor (TNF) production was assessed by flow cytometry (fig. S16). Moreover, in vitro PD-L1 blockade was not associated with a generalized increase in proinflammatory cytokine production by PBMCs from critical COVID-19 patients (fig. S17).

DISCUSSION

In this work, we report that PD-1/PD-L1 blockade overcomes inflammasome-dependent T cell dysfunction in critical β-coronavirus disease. We show a conserved pathogenic process that relates innate and adaptive immune dysfunction in critical β-coronavirus disease. Specifically, we linked inflammasomes to T cell exhaustion in infection by two β-coronaviruses, SARS-CoV-2 and MHV-A59. Moreover, TMEM176B was identified as a key regulator in this pathway. Our results help us understand how T cell dysfunction is regulated by inflammation while providing a mechanistic basis that supports a pathogenic role for inflammasomes in β-coronavirus disease.
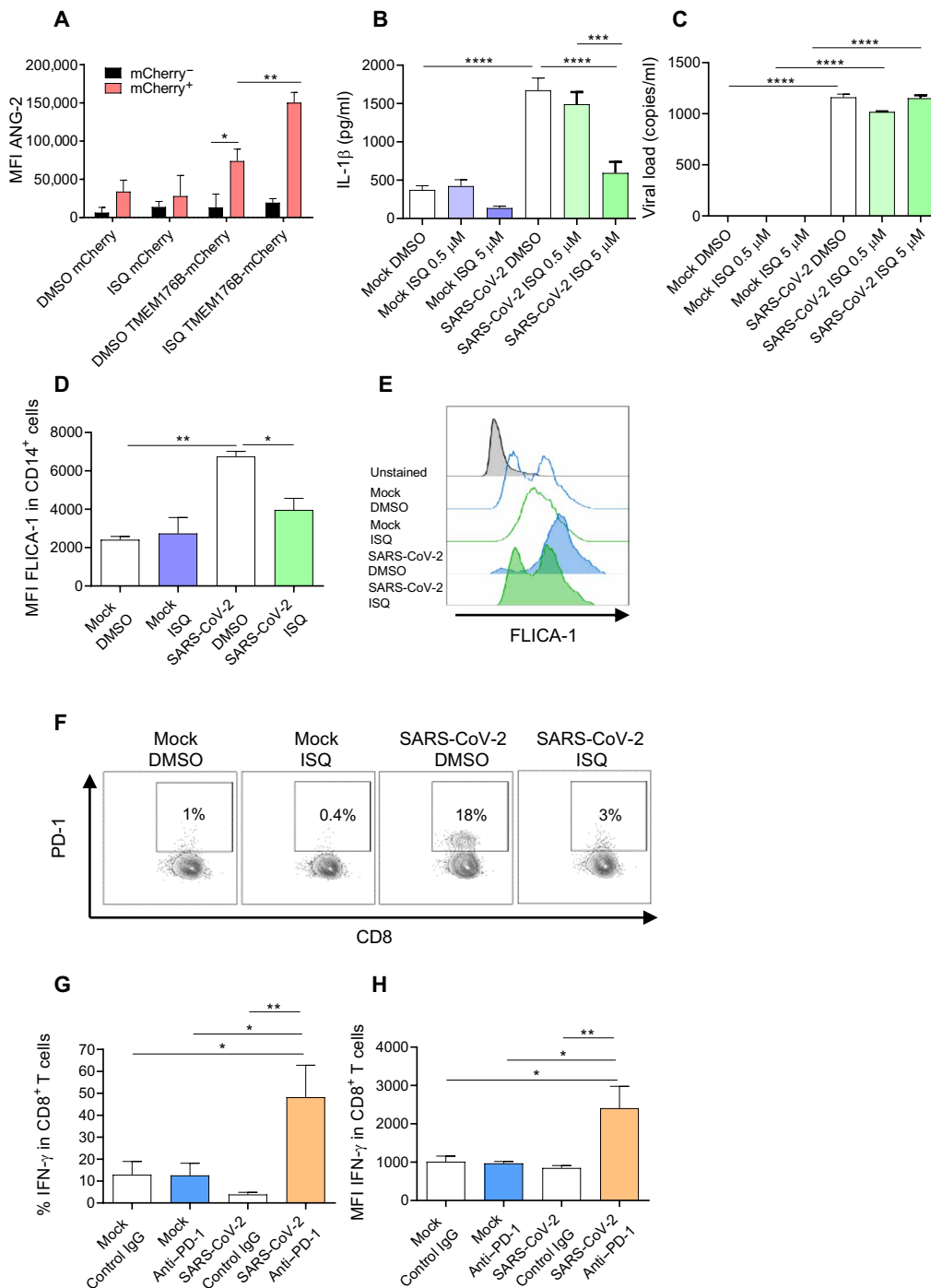
Fig. 3. Pharmacological modulation of the inflammasome/dysfunctional T cell axis triggered by SARS-CoV-2 in vitro. (**A**) Flow cytometry study of *TMEM176B*-dependent Na^+ transport in CHO cells loaded with the Na^+-sensitive probe Asante NaTRIUM Green-2 (ANG-2). Cells were treated with 5 μM of the flavonoid isoquercetin (ISQ) or dimethyl sulfoxide (DMSO; vehicle control). MFI, mean fluorescence intensity. One experiment representative of four is shown. *$P < 0.05$; **$P < 0.01$, two-way ANOVA test. (**B**) Study of IL-1β secretion by human primary monocytes infected with SARS-CoV-2 ± ISQ. Mock, not infected. One experiment representative of three is shown. ***$P < 0.001$; ****$P < 0.0001$, one-way ANOVA test. (**C**) Study of viral load in human primary monocytes infected with SARS-CoV-2 ± 5 μM ISQ. One experiment representative of three is shown. ****$P < 0.0001$, one-way ANOVA test. (**D**) Study of FLICA-1 MFI (active caspase-1) from a pool of three independent experiments, where human primary monocytes were not infected (Mock) or infected with SARS-CoV-2 and treated with DMSO (vehicle control) or with 5 μM ISQ. *$P < 0.05$; **$P < 0.01$, one-way ANOVA test. (**E**) Representative flow cytometry histograms of the experiments shown in (D). One experiment representative of three is shown. (**F**) Study of PD-1 expression by CD8$^+$ TCR-β$^+$ cells cocultured with allogeneic monocytes ± cell culture medium (CCM) from SARS-CoV-2–infected monocytes ± 5 μM ISQ. One experiment representative of three is shown. (**G** and **H**) Flow cytometry study of IFN-γ expression by CD8$^+$ T cells cocultured with allogeneic monocytes ± CCM from uninfected monocytes (Mock) or SARS-CoV-2–infected cells ± anti–PD-1 or control antibody (20 μg/ml). The percentage of IFN-γ$^+$ cells is shown in (G), and the MFI of positive cells is shown in (H). The graphics show one experiment representative of three. *$P < 0.05$; **$P < 0.01$, one-way ANOVA test.
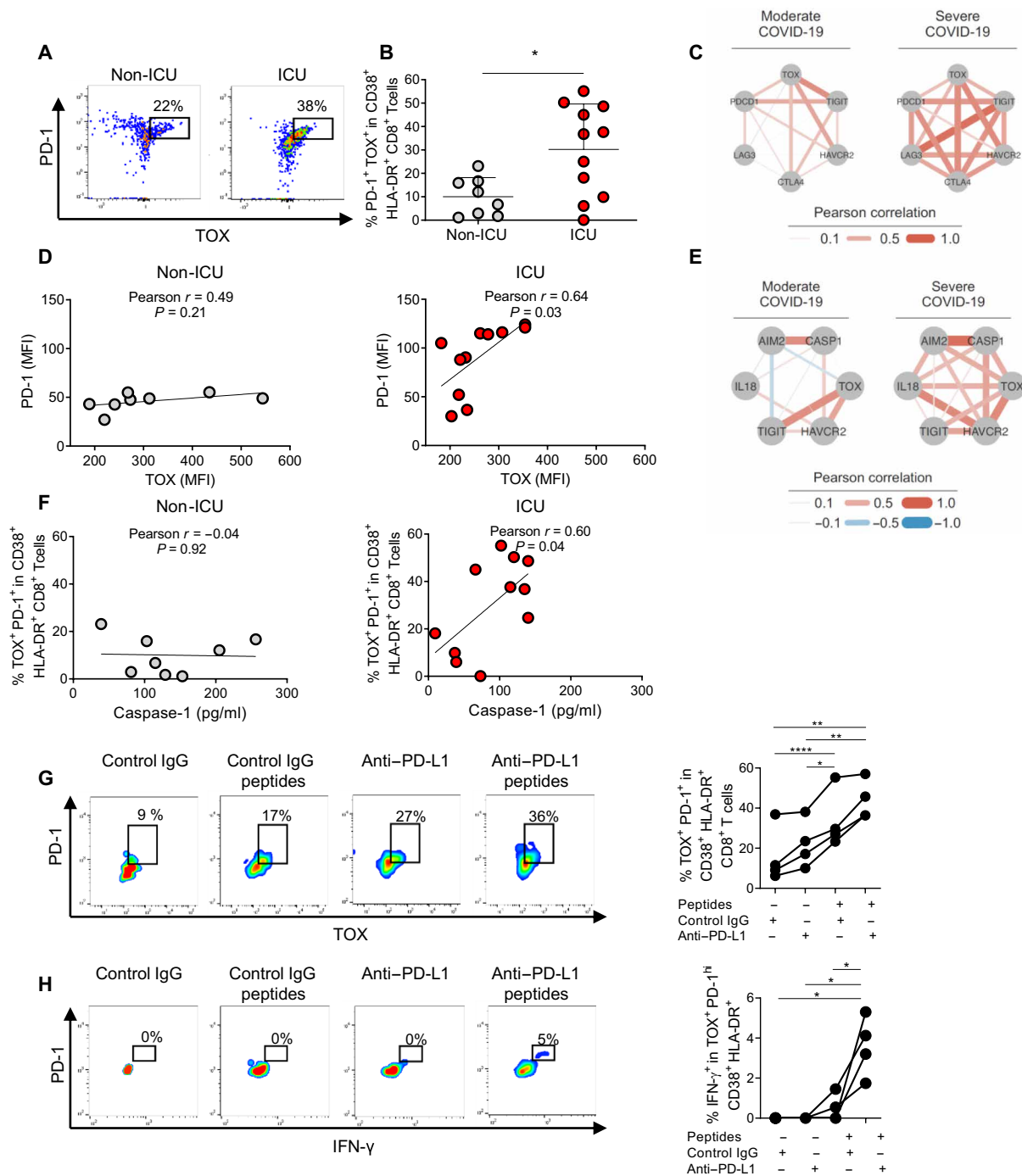
Fig. 4. Exhausted T cells correlate with plasmatic active caspase-1 in critical COVID-19 and can be modulated by anti–PD-L1 antibodies. (**A**) Representative dot plots of a flow cytometry study of PD-1 and TOX in CD8^{+} TCR-β^{+} CD38^{+} HLA-DR^{+} cells in non-ICU and ICU patients. (**B**) The graphic shows the individual percentages of PD-1^{+} TOX^{+} cells within CD38^{+} HLA-DR^{+} CD8^{+} TCR-β^{+} for each studied patient. *$P < 0.05$, Student's t test. (**C**) Network plot representing Pearson correlations of the indicated genes. Transcriptomic data from peripheral blood were analyzed from McClain *et al.* (*46*). (**D**) Correlation study between the MFI determined by flow cytometry of PD-1 and TOX within CD8^{+} TCR-β^{+} CD38^{+} HLA-DR^{+} cells in non-ICU and ICU patients. (**E**) Network plot representing Pearson correlations of the indicated genes. Transcriptomic data from peripheral blood were analyzed from McClain *et al.* (*46*). (**F**) Correlation study between the percentage of PD-1^{+} TOX^{+} cells in CD8^{+} TCR-β^{+} CD38^{+} HLA-DR^{+} cells and plasmatic active caspase-1 in non-ICU and ICU patients. (**G**) Flow cytometry study of the percentage of PD-1^{+} TOX^{+} cells within CD38^{+} HLA-DR^{+} CD8^{+} T cells from four lymphopenic ICU patients. Cells were incubated for 24 hours with control IgG (20 μg/ml; human IgG1) or anti–PD-L1 antibody. Then, 6 nmol of SARS-CoV-2 peptides was added or not to the culture for 6 hours. Representative dot plots are shown in the left panel. Data for the four studied patients are shown in the right panel. *$P < 0.05$; **$P < 0.01$; ****$P < 0.0001$, one-way ANOVA test. (**H**) Flow cytometry study of IFN-γ production by CD8^{+} TCR-β^{+} CD38^{+} HLA-DR^{+} PD-1^{+} TOX^{+} cells from the same ICU patients studied in (G) under the same in vitro treatments. Representative dot plots are shown in the left panel. Data for the four studied patients are shown in the right panel. *$P < 0.05$, one-way ANOVA test.

Although MHV-A59 and SARS-CoV-2 are β-coronaviruses, they are still very different viruses. Thus, the common findings involving both viruses highlight a conserved pathogenic mechanism and therapeutic response. Active plasma caspase-1 and IL-18 levels have been associated with disease severity (47). Moreover, IL-1 receptor blockade led to improved overall and mechanical ventilation-free survival in severe but not mild-to-moderate COVID-19 patients (48–50). However, it was recently shown that blockade of IL-1β and IL-18 resulted in increased mortality in SARS-CoV-2–infected transgenic hACE2 mice, suggesting that these inflammasome-related cytokines may play a protective role in this model (51). These results seem to contradict our observations as well as clinical outcomes obtained with IL-1 receptor antagonists. Nevertheless, the relevance of the hACE2 model to the study of inflammasome activation has been questioned (2, 3). Specifically, the fact that the transgene is not expressed by leukocytes (52) is a clear difference from natural SARS-CoV-2 infection in humans. Thus, the lack of leukocyte infection in hACE2 animals may not completely reproduce inflammasome activation in COVID-19 patients. Moreover, SARS-CoV-2 infection of hACE2 transgenic mice does not recapitulate the multiorgan viral spread seen in COVID-19 patients, whereas the MHV-A59 infection model does (2, 38).

Although T cell exhaustion has been classically associated with chronic viral infections, it is important to state that exhausted T cells can arise within a few days of infections with viral strains that result in chronic infections (45). Our results suggest that in a strong acute inflammatory environment, particularly with unleashed inflammasome activation, the clinical outcome of coronavirus disease can be worsened through mechanisms dependent on the generation of T cell exhaustion. Similarly, acute hyperinflammation in sepsis has also been proposed to be associated with exhausted T cells (53–55). Nevertheless, because only a 24-hour incubation with anti–PD-L1 blockers rescued T cell functionality, it is possible that the exhaustion status is not fully established in critical COVID-19 patients. However, we propose that PD-1/PD-L1 blockade may add clinical benefit in acute critical COVID-19. In clinical settings, although prior PD-1 blockade in cancer patients suffering from COVID-19 may improve T cell functionality against SARS-CoV-2 antigens (56), this therapy has not been shown to improve the clinical outcome of the viral disease when administered before infection (28, 57). Moreover, therapy with immune checkpoint blockers before infection was a predictor of hospitalization and severe COVID-19 in an observational study including 423 cancer patients (58). Thus, whether cancer patients being treated with PD-1/PD-L1 blockers that are infected with SARS-CoV-2 may obtain some benefit in COVID-19 outcome needs further research. Because PD-1/PD-L1 blockade may exacerbate the cytokine storm in severely ill patients, it has been suggested that clinical studies assessing anti–PD-1/PD-L1 therapy in COVID-19 should focus on mild disease (28). However, the pathogenic mechanisms reported here contradict this view. Our results in mice and in peripheral blood samples from COVID-19 patients add evidence supporting the use of PD-1/PD-L1 blockade therapy in critical β-coronavirus disease. However, there is a reasonable concern that PD-1/PD-L1 blockade in a hyperinflammatory scenario may lead to immunopathology. Nevertheless, a phase 1b clinical trial has shown that PD-1/PD-L1 blockade in sepsis is safe (59).

In conclusion, our study highlights a novel therapeutic strategy for COVID-19 based on the repurposing of a current cancer immunotherapy. This strategy is mechanistically supported by T cell dysfunction driven by TMEM176B-unleashed inflammasomes in critical disease.

MATERIALS AND METHODS
Reagents and kits
ISQ was from Quercegen Pharmaceuticals LLC. Nigericine, adenosine triphosphate (ATP), and lipopolysaccharides from *Escherichia coli* 0111:B4 were from Sigma-Aldrich. DDAO-SE [7-hydroxy-9H-(1,3-dichloro-9,9-dimethylacridin-2-one)] and Lipofectamine 2000 were from Thermo Fisher Scientific. FLICA 660 Caspase-1 Assay (FLICA-1) was from Immunochemistry. Random primers, TRIzol Reagent, and M-MLV Reverse Transcriptase were purchased to Invitrogen. Fast SYBR Green Master Mix was from Applied Biosystems. Active (p20) human caspase-1 kit was from R&D Systems. IL-1β levels were measured by enzyme-linked immunosorbent assay (ELISA) (BD OptEIA kit, BD Biosciences, San Jose, CA; 559603). Human CD14 positive selection kit, mouse CD8 negative selection kit, and CD11c positive selection kit were from Miltenyi. GPT quantification kit was from Human Diagnostics worldwide. PepTivator SARS-Cov-2 Prot_S P1 and Prot_S B1.1.529 Mutation Pools and PepTivator SARS-CoV-2 Select were from Miltenyi.

Viruses
MHV-A59 was provided by L. Retegui (UBA-CONICET, Argentina). MHV-A59 viruses were expanded in murine L929 cells [American Type Culture Collection (ATCC)] to a concentration of 1×10^7 plaque-forming units (PFU)/ml. The virus-containing supernatants were stored at −80°C until use.

HIAE-02 SARS-CoV-2/SP02/human/2020/BRA (GenBank accession number MT126808.1) virus was isolated from the second confirmed case in Brazil and donated by E. L. Durigon. SARS-CoV-2 virus stocks were propagated in the Vero cell line, and supernatant was harvested at 2 to 3 dpi. The viral titers were determined by plaque assays on Vero cells. Vero CCL-81 cells were cultivated in minimum essential medium (MEM) supplemented with 10% heat-inactivated fetal bovine serum (FBS) and 1% penicillin-streptomycin and incubated at 37°C with 5% CO_2 atmosphere.

Cells
BMDCs were generated from BM precursors from male and female C57BL/6 mice. BM cells from WT, *Tmem176b*$^{-/-}$, and *Tmem176b*$^{-/-}$ *Casp1*$^{-/-}$ animals were cultured for 8 days in the presence of low doses of granulocyte-macrophage colony-stimulating factor (GM-CSF) (0.4 ng/ml) (31). By day 8, adherent cells were harvested and used for in vitro experiments. BMDCs were >95% CD11c$^+$ CD11b$^+$ MHC II^{int}. BMDCs were infected with MHV-A59 at different MOIs (multiplicities of infection) in vitro. Human THP-1 monocytes (TIB-202) and Chinese hamster CHO-K1 (CCL-61) cell lines were purchased from ATCC (Manassas, VA).

In vitro inflammasome activation
BMDCs were infected with MHV-A59 and human primary monocytes with SARS-CoV-2 for 24 hours. THP-1 monocytes were transfected with plasmid coding for envelope (E) protein from SARS-CoV-2 or control [green fluorescent protein (GFP)] plasmid. The presence of IL-1β was assessed in culture supernatants by ELISA (BioLegend, 432603; R&D Systems, Human IL-1β/IL-1F2 DuoSet ELISA). To determine caspase-1 activation, BMDCs, THP-1

cells, and primary human monocytes were stained with FLICA-1 and analyzed by flow cytometry.

THP-1 transfection and inflammasome activation
THP-1 monocytes were nucleofected with the GFP or SARS-CoV-2–E protein–GFP coding pcDNA3.1 plasmids using the Amaxa Cell Line Nucleofector Kit V-Lonza and Nucleofector 2b Device (Amaxa). In another set of experiments, THP-1 monocytes were cotransfected with SARS-CoV-2–E protein–GFP–pcDNA3.1 and pmCherry-N1 or TMEM176B-pmCherry-N1 plasmids. Sixteen hours later, cells were treated for 24 hours with lipopolysaccharide (0.25 µg/ml). Supernatants were collected to determine IL-1β by ELISA, and cell viability was assessed by flow cytometry using DAPI (4′,6-diamidino-2-phenylindole).

Mice and experimental design
ARRIVE guidelines were followed for experimental research using mice. All animal protocols were approved by the institutional animal care and use committee of Institut Pasteur Montevideo (006-21). All mice in this study are on the C57BL/6 background, female and male, 8 to 10 weeks old. Sample size was determined using G*Power software (www.gpower.hhu.de). Mice were randomly distributed into experimental groups. *Tmem176b*$^{-/-}$ mice were generated in the 129/SvJ strain, and heterozygous mice were back-crossed for 10 generations onto the C57BL/6 background (Janvier, Saint Berthevin, France) as reported (*31*). *Tmem176b*$^{-/-}$*Casp1*$^{-/-}$ mice were generated as previously described through CRISPR-Cas9 technology (*31*). *Nlrp3*$^{-/-}$ (B6.129S6-Nlrp3tm1Bhk/J; 021302) and *Casp1/11*$^{-/-}$ (B6N.129S2-Casp1tm1Flv/J; 016621) were from The Jackson Laboratory (Bar Harbor, ME). *Nlrp3*$^{-/-}$ animals were compared to 000664 C57BL/6J and *Casp1/11*$^{-/-}$ mice to 005304 C57BL/6NJ. Mice were maintained in micro-isolator cages (IsoCageN, Techniplast, Milano, Italy), with autoclaved water and food (5K67 LabDiet, PMI Nutrition International, USA) supplied ad libitum and housed in the animal facility at the Institut Pasteur Montevideo. In in vivo experiments, *Casp1/11*$^{-/-}$ mice were intraperitoneally injected with 1200 PFU of MHV-A59 and *Tmem176b*$^{-/-}$ mice were injected with 800 PFU. In neutralization experiments, mice were treated with anti–IL-1β antibody (R&D Systems, Minneapolis, MN; clone AF-401-NA; 1 µg/5 days since day −2) or anti–PD-1 (clone RMP1-14 BP0146, Bio X Cell, West Lebanon, NH) (200 µg intraperitoneally/3 days) or rat IgG2a control antibody (clone 2A3 BP0089, Bio X Cell) or anti-CD8a (clone YTS169.4 BE0117, Bio X Cell; RRID:AB_10950145) (100 µg intraperitoneally/3 days from day −2) in depletion experiments. Mice were euthanized by cervical dislocation on the indicated days to obtain samples. Blinded processing of the samples and analysis of data were performed.

Western blot analysis
Liver extracts (50 µg of protein) were submitted to 12% SDS–polyacrylamide gel electrophoresis and then transferred onto nitrocellulose sheets (GE Life Sciences, Pittsburg, PA). After transfer, nonspecific antibody-binding sites were blocked with 3% bovine serum albumin, 30 mM tris, 0.14 M NaCl, and 0.1% (v/v) Tween 20 (pH 8.0) for 1 hour at room temperature with shaking. Specific antibody incubation was overnight at 4°C (anti–IL-1β, clone H-153, sc-7884, Santa Cruz Biotechnology, Dallas, TX; RRID:AB_2124476; anti–caspase-1, AdipoGen Life Sciences, San Diego, CA; clone gasper-1; RRID:AB_2755041). Bound antibody was revealed with

peroxidase-labeled anti-mouse (115-035-003, Jackson Immuno Research, West Grove, PA; RRID:AB_10015289) or anti-rabbit (111-035-003, Jackson ImmunoResearch, West Grove, PA; RRID:AB_2313567) and Pierce ECL reagent (Thermo Fisher Scientific, Waltham, MA). Human CD14$^+$ monocytes were studied with anti-TMEM176B (Abcam, 103929, rabbit polyclonal antibody; RRID:AB_10712259).

In vivo cytotoxic T lymphocyte assay
The assay was described previously (*31*). Briefly, splenocytes from naive mice were stained with DDAO. Control target cells were labeled with a low concentration of DDAO (0.08 µM), whereas target cells loaded with MHV-A59–specific peptide (RCQIFANI, S598-605) were labeled with a 10-fold concentration of DDAO (0.8 µM). The two cell populations are then mixed in equal numbers and transferred intravenously into syngeneic mice infected with MHV-A59 5 days before. Animals were euthanized 4 hours later, and cell suspensions were made from spleen and analyzed. The cell suspensions are then assessed by flow cytometry for the proportions of transferred cells. The % specific lysis was calculated as follows: % specific lysis = $(1-[r_{naive}/r_{infected}]) \times 100$, where r = %DDAO$_{low}$ cells / %DDAO$_{high}$ cells.

TMEM176B activity assay
CHO cells were transfected with pmCherry-N1 or huTMEM176b-pmCherry-N1 plasmids using Lipofectamine LTX with Plus Reagent for 4 hours, washed, and cultured for 24 hours. Cells were then loaded with 1 mM ANG-2 (Asante NaTRIUM Green-2) for 30 min at 37°C, washed, and incubated for 30 min in 140 mM Na$^+$-containing phosphate buffer or 140 mM N-methyl-D-glucamine (NMDG) to substitute Na$^+$ in the presence of different doses of tested drugs or vehicle controls. Cells were then analyzed by flow cytometry using a BD Accuri C6 cytometer equipped with a 488-nm laser. ANG-2 emission was detected using a 530/30-nm band-pass filter, and mCherry was determined using a 670-nm long-pass filter. FlowJo vX.0.7 software was used for data analysis. MFI from NMDG-containing solutions was subtracted to MFI from Na$^+$-containing solutions.

Flow cytometry
Caspase-1 activity from virus-infected BMDCs was determined using FLICA 660 Caspase-1 Assay (ImmunoChemistry Technologies, Bloomington, MN). For in vivo determination of CD8$^+$ T cell infiltration, the following antibodies were used: anti-mouse CD8a (clone 53-6.7, 100714, BioLegend; RRID:AB_312753), anti-mouse T cell receptor (TCR) β chain (clone H57-597, 109226, BioLegend; RRID:AB_1027649), anti-mouse TCF-1 (clone C63D9, 6444S, Cell Signaling), anti-mouse TOX (clone TXRX10, 50-6502-82, Invitrogen), anti-mouse/human CD44 (clone 30-F11, 103147, BioLegend; RRID:AB_256245), and anti-mouse CD279 (clone J43, 109110, BioLegend; RRID:AB_572017). Total liver and spleen recovered cells were stained with the indicated antibody for 20 min at 4°C in phosphate-buffered saline (PBS)–0.2% FBS–0.1% sodium azide. Cells were washed two times with PBS–0.2% FBS–0.1% sodium azide and then analyzed using BD Aria FUSION (BD Biosciences) or CyAn ADP (Beckman Coulter) flow cytometer. For MHV-specific CD8$^+$ T cell analysis, phycoerythrin (PE)–conjugated tetramers (RCQIFANI, S598–605, H-2Kb) prepared by the National Institutes of Health (NIH) Tetramer Core Facility (Emory University, Atlanta, GA) were used. Total liver cells were stained with PE-conjugated tetramer (1:100 dilution). Flow cytometry data were analyzed using FlowJo software (Tree Star, Ashland, OR).

Human PBMCs were stained with anti-TCR α/β (clone IP26, 351708, BioLegend; RRID:AB_10612569), anti-CD8 (clone RPA-T8, 344714, BioLegend; RRID:AB_2044006), anti-HLA-DR (clone L243, 307616, BioLegend; RRID:AB_493588), anti–PD-1 (clone EH12.2H7, 329916, BioLegend; RRID:AB_2283437), anti-CD38 (clone HIT2, 303504, BioLegend; RRID:AB_314356), anti-TOX (clone REA473, 130-120-785, Miltenyi), REA control antibody (I) human IgG1 (130-118-147, Miltenyi), anti–IFN-γ (clone B27, 506541, Bio-Legend; RRID:AB_2801101), anti-TNF (clone Mab11, 502928, Bio-Legend; RRID:AB_2561315), and mouse IgG1 κ isotype control (clone MOPC-21, 400144, BioLegend). Cytokines in the culture supernatant were quantified using a bead-based multiplex kit from BioLegend (740809, LegendPlex Human Inflammation Panel 1).

Quantitative real-time polymerase chain reaction in mouse studies

Total RNA was isolated with TRI Reagent (Sigma-Aldrich, St. Louis, MO) from spleen and liver. Samples were analyzed in the Eco Real-Time PCR System (Illumina, San Diego, CA) using Fast SYBR Green Master Mix (Thermo Fisher Scientific). The reactions were performed according to the following settings: 95°C for 10 min and 40 cycles of 95°C for 15 s, followed by cycles of 60°C for 1 min. The following primers were used: MHV, GGAACTTCTCGTTGGG-CATTATACT (forward) and ACCACAAGATTATCATTTTCA-CAACATA (reverse).

Immunofluorescence staining

Mouse liver cryosections (20 μm) were fixed in acetone, and the staining procedure used blocking buffer, followed by primary antibody stainings (anti-TMEM176B, Proteingroup, 19825-1; anti–MHC II, Serotec, MCA45R) and secondary antibodies (Alexa Fluor 488 goat anti-mouse, Invitrogen, A-11029, or biotinylated anti-rabbit, Sigma-Aldrich, SAB3700936/streptavidin, Alexa Fluor 568 conjugate, Thermo Fisher Scientific, S11226). Sections were washed three times with PBS after each of the incubations. Nuclei were counterstained using DAPI. For negative controls, we incubated sections with isotype immunoglobulin G (IgG) control or PBS instead of primary antibodies. Images were acquired using an LSM 880 confocal microscope and Zen blue microscopy software (Zeiss).

Patients and HDs

All patients had a positive polymerase chain reaction (PCR) test for SARS-CoV-2. They were enrolled in accordance with the Institutional Review Board of CASMU and Sanatorio Americano (IPM-COVID19-001) and with the principles of the Declaration of Helsinki. Informed consent was obtained from patients and HDs after the nature and possible consequences of the studies were explained. HDs had a negative PCR test for SARS-CoV-2 and were negative for anti–SARS-CoV-2 antibodies. Patients and donors were not vaccinated against SARS-CoV-2. PBMCs were isolated with Ficoll/Hypaque density gradient centrifugation. CD14^{+} cells were enriched using a CD14 human positive selection kit from Miltenyi. Enrichments were typically >80%.

Buffy coats from Unicamp's Hematology and Hemotherapy Center (SP-Campinas, Brazil) were used to isolate PBMCs. Buffy coats were diluted (1:1) with PBS. Twenty-five milliliters of mixture was carefully transferred to a 50-ml tube containing 7.5 ml of Ficoll, which was centrifuged at 2700 rpm for 20 min at room temperature,

without breaking. The layers of PBMCs were collected with a pipette and transferred to a new 50-ml tube and washed with PBS. The pellet was then incubated with a lysis buffer for 5 min for red blood cell removal and then washed with PBS. Total PBMCs were cultured as adherent monolayers (1.5×10^6 cells/ml) in RPMI 1640 supplemented with 1% penicillin-streptomycin. After 2 to 3 hours of adhesion, cells were washed with PBS and incubated until infection with RPMI 1640 containing 10% FBS and 1% penicillin-streptomycin at 37°C with 5% CO_2 atmosphere. This study was approved by the Brazilian Committee for Ethics in Human Studies (CAEE 31622420.0.0000.5404).

Charlson comorbidity index was calculated using www.mdcalc.com/charlson-comorbidity-index-cci. World Health Organization clinical progression scale (WHO-CPS) score was used as reported by the WHO Working Group on the Clinical Characterisation and Management of COVID-19 infection (60).

Human lymphocyte isolation and mixed lymphocyte reaction

PBMCs isolated from buffy coats of healthy volunteers were used. Briefly, 5×10^5 cells were cocultured with 0.5×10^5 cells from another patient to allogenic reaction. The cells were incubated with pembrolizumab (20 μg/ml) or IgG control or with different conditioned media. After 72 hours, cells were stimulated with phorbol 12-myristate 13-acetate (0.1 μg/ml) and calcium ionophore (0.5 μg/ml) (A23187) in the presence of brefeldin A (10 μg/ml) for 4 hours. Cells were transferred to a clean conical 96-well plate, centrifuged at 2000 rpm for 5 min, and labeled with fixable viability stain, anti-CD3–BV421, anti-CD8–PECy7, and anti-CD4–APC (allophycocyanin) in PBS + 2% FBS for 20 min on ice. One hundred microliters of PBS + 2% FBS were added, and the cells were centrifuged at 2000 rpm for 5 min. Cells were permeabilized for 20 min using the Fixation/Permeabilization Kit (BD) and washed with Perm Wash buffer. The cells were incubated with anti–IFN-γ–BV605. Cells were then acquired by flow cytometry (FACSymphony, Becton & Dickinson, San Diego, CA, USA) and analyzed using FlowJo software.

Reagents and infection with SARS-CoV-2

Cells were infected with mock control or SARS-CoV-2 (MOI 0.1) under continuous agitation at 15 rpm for 1 hour for virus absorption. After infection, cells were washed twice with prewarmed PBS. Cells were incubated with ISQ (0.5 and 5 μM) in RPMI containing 10% FBS and 1% penicillin-streptomycin for 24 hours at 37°C with 5% CO_2 atmosphere.

RNA extraction, viral load, and gene expression analyses in SARS-CoV-2 experiments

Total RNA extractions were performed using TRIzol Reagent according to the manufacturer's instructions. RNA concentration was determined with a NanoDrop 2000 spectrophotometer (Thermo Fisher Scientific). Extracted total RNA was reverse-transcribed using a GoScript Reverse Transcriptase cDNA synthesis kit according to the manufacturer's instructions. For viral load detection, we used specific SARS-CoV-2 N1 primers targeting the N1 region. Standard curve was generated using serial dilutions of SARS-CoV-2. Viral load and gene expression quantitative reverse transcription PCR (qRT-PCR) were performed using SYBR Green Supermix. All qRT-PCRs were performed using the Bio-Rad CFX394 Touch Real-Time PCR Detection System on 384-well plates.

Human IL-1β ELISA

IL-1β levels were measured in the supernatant of PBMCs infected or not with SARS-CoV-2 following the manufacturer's instructions (R&D Systems, Human IL-1β/IL-1F2 DuoSet ELISA).

Generation of conditioned medium

Conditioned medium was generated by incubating PBMCs with mock control or SARS-CoV-2 as described previously. Supernatant from each condition was collected and placed under ultraviolet light for 30 min for residual virus inactivation. Supernatants were stored in −80°C until use in human T cell experiments.

In vitro stimulation of PBMCs with SARS-CoV-2 peptides

Two million cells per well were seeded in U-bottom 96-well microplates in RPMI culture medium complemented with 10% autologous serum. Anti–PD-L1 or control human IgG1 was added at 20 μg/ml. Twenty-four hours later, 0.6 nmol of each peptide was incubated for 6 hours from a pool of SARS-CoV-2 peptides from M, N, E, and S WT proteins and from P.1 or Omicron S protein. Brefeldin A (1 μg/ml) was added for the last 4 hours of culture. Exhausted T cells, IFN-γ, and TNF production were studied by flow cytometry.

Anti–SARS-CoV-2 antibody ELISA

Specific IgG levels against the receptor-binding domain (RBD) of SARS-CoV-2 Spike were determined in plasma samples from HDs, non-ICU patients, and ICU patients by using the COVID-19 IgG QUANT ELISA Kit (developed by Universidad de la República, Institut Pasteur Montevideo and ATGen Company), according to the manufacturer's instructions. Quantitative test results were expressed in binding antibody units per milliliter, referred to the First WHO International Standard for anti–SARS-CoV-2 immunoglobulin (NIBSC code: 20/136) used for test calibration.

Statistical analysis

Statistical significance was evaluated using either one-way analysis of variance (ANOVA), two-way ANOVA, Student's *t* test, or Mann-Whitney test as indicated in the figure legends. When the experimental design included three or more groups, ANOVA test was used. Survival curves were compared with the log-rank (Mantel-Cox) test. All statistical analyses were performed using GraphPad Prism 7.0 (GraphPad Software, San Diego, CA).

SUPPLEMENTARY MATERIALS

Supplementary material for this article is available at https://science.org/doi/10.1126/sciadv.abn6545

View/request a protocol for this paper from *Bio-protocol*.

REFERENCES AND NOTES

1. C. D. Camell, M. J. Yousefzadeh, Y. Zhu, L. G. P. L. Prata, M. A. Huggins, M. Pierson, L. Zhang, R. D. O'Kelly, T. Pirtskhalava, P. Xun, K. Ejima, A. Xue, U. Tripathi, J. M. Espindola-Netto, N. Giorgadze, E. J. Atkinson, C. L. Inman, K. O. Johnson, S. H. Cholensky, T. W. Carlson, N. K. LeBrasseur, S. Khosla, M. G. O'Sullivan, D. B. Allison, S. C. Jameson, A. Meves, M. Li, Y. S. Prakash, S. E. Chiarella, S. E. Hamilton, T. Tchkonia, L. J. Niedernhofer, J. L. Kirkland, P. D. Robbins, Senolytics reduce coronavirus-related mortality in old mice. *Science* **373**, eabe4832 (2021).

2. S. Grabherr, B. Ludewig, N. B. Pikor, Insights into coronavirus immunity taught by the murine coronavirus. *Eur. J. Immunol.* **51**, 1062–1070 (2021).

3. S. Lee, R. Channappanavar, T.-D. Kanneganti, Coronaviruses: Innate immunity, inflammasome activation, inflammatory cell death, and cytokines. *Trends Immunol.* **41**, 1083–1099 (2020).

4. A. Sariol, S. Perlman, Lessons for COVID-19 immunity from other coronavirus infections. *Immunity* **53**, 248–263 (2020).

5. M. Zheng, R. Karki, E. P. Williams, D. Yang, E. Fitzpatrick, P. Vogel, C. B. Jonsson, T.-D. Kanneganti, TLR2 senses the SARS-CoV-2 envelope protein to produce inflammatory cytokines. *Nat. Immunol.* **22**, 829–838 (2021).

6. S. Ryu, I. Shchukina, Y.-H. Youm, H. Qing, B. Hilliard, T. Dlugos, X. Zhang, Y. Yasumoto, C. J. Booth, C. Fernández-Hernando, Y. Suárez, K. Khanna, T. L. Horvath, M. O. Dietrich, M. Artyomov, A. Wang, V. D. Dixit, Ketogenic diet restrains aging-induced exacerbation of coronavirus infection in mice. *eLife* **10**, e66522 (2021).

7. T. S. Rodrigues, K. S. G. de Sá, A. Y. Ishimoto, A. Becerra, S. Oliveira, L. Almeida, A. V. Gonçalves, D. B. Perucello, W. A. Andrade, R. Castro, F. P. Veras, J. E. Toller-Kawahisa, D. C. Nascimento, M. H. F. de Lima, C. M. S. Silva, D. B. Caetite, R. B. Martins, I. A. Castro, M. C. Pontelli, F. C. de Barros, N. B. do Amaral, M. C. Giannini, L. P. Bonjorno, M. I. F. Lopes, R. C. Santana, F. C. Vilar, M. Auxiliadora-Martins, R. Luppino-Assad, S. C. L. de Almeida, F. R. de Oliveira, S. S. Batah, L. Siyuan, M. N. Benatti, T. M. Cunha, J. C. Alves-Filho, F. Q. Cunha, L. D. Cunha, F. G. Frantz, T. Kohlsdorf, A. T. Fabro, E. Arruda, R. D. R. de Oliveira, P. Louzada-Junior, D. S. Zamboni, Inflammasomes are activated in response to SARS-CoV-2 infection and are associated with COVID-19 severity in patients. *J. Exp. Med.* **218**, e20201707 (2021).

8. D. Mathew, J. R. Giles, A. E. Baxter, D. A. Oldridge, A. R. Greenplate, J. E. Wu, C. Alanio, L. Kuri-Cervantes, M. B. Pampena, K. D'Andrea, S. Manne, Z. Chen, Y. J. Huang, J. P. Reilly, A. R. Weisman, C. A. G. Ittner, O. Kuthuru, J. Dougherty, K. Nzingha, N. Han, J. Kim, A. Pattekar, E. C. Goodwin, E. M. Anderson, M. E. Weirick, S. Gouma, C. P. Arevalo, M. J. Bolton, F. Chen, S. F. Lacey, H. Ramage, S. Cherry, S. E. Hensley, S. A. Apostolidis, A. C. Huang, L. A. Vella; UPenn COVID processing unit, M. R. Betts, N. J. Meyer, E. J. Wherry, Deep immune profiling of COVID-19 patients reveals distinct immunotypes with therapeutic implications. *Science* **369**, eabc8511 (2020).

9. C. Rydyznski Moderbacher, S. I. Ramirez, J. M. Dan, A. Grifoni, K. M. Hastie, D. Weiskopf, S. Belanger, R. K. Abbott, C. Kim, J. Choi, Y. Kato, E. G. Crotty, C. Kim, S. A. Rawlings, J. Mateus, L. P. V. Tse, A. Frazier, R. Baric, B. Peters, J. Greenbaum, E. Ollmann Saphire, D. M. Smith, A. Sette, S. Crotty, Antigen-specific adaptive immunity to SARS-CoV-2 in acute COVID-19 and associations with age and disease severity. *Cell* **183**, 996–1012.e19 (2020).

10. Y. Liu, L.-M. Yan, L. Wan, T.-X. Xiang, A. Le, J.-M. Liu, M. Peiris, L. L. M. Poon, W. Zhang, Viral dynamics in mild and severe cases of COVID-19. *Lancet Infect. Dis.* **20**, 656–657 (2020).

11. J. H. Stone, M. J. Frigault, N. J. Serling-Boyd, A. D. Fernandes, L. Harvey, A. S. Foulkes, N. K. Horick, B. C. Healy, R. Shah, A. M. Bensaci, A. E. Woolley, S. Nikiforow, N. Lin, M. Sagar, H. Schrager, D. S. Huckins, M. Axelrod, M. D. Pincus, J. Fleisher, C. A. Sacks, M. Dougan, C. M. North, Y.-D. Halvorsen, T. K. Thurber, Z. Dagher, A. Scherer, R. S. Wallwork, A. Y. Kim, S. Schoenfeld, P. Sen, T. G. Neilan, C. A. Perugino, S. H. Unizony, D. S. Collier, M. A. Matza, J. M. Yinh, K. A. Bowman, E. Meyerowitz, A. Zafar, Z. D. Drobni, M. B. Bolster, M. Kohler, K. M. D'Silva, J. Dau, M. M. Lockwood, C. Cubbison, B. N. Weber, M. K. Mansour; BACC bay tocilizumab trial investigators, Efficacy of tocilizumab in patients hospitalized with covid-19. *N. Engl. J. Med.* **383**, 2333–2344 (2020).

12. O. Hermine, X. Mariette, P.-L. Tharaux, M. Resche-Rigon, R. Porcher, P. Ravaud; CORIMUNO-19 Collaborative Group, Effect of tocilizumab vs usual care in adults hospitalized with COVID-19 and moderate or severe pneumonia: A randomized clinical trial. *JAMA Intern. Med.* **181**, 32–40 (2021).

13. The REMAP-CAP Investigators, Interleukin-6 receptor antagonists in critically ill patients with covid-19. *N. Engl. J. Med.* **384**, 1491–1502 (2021).

14. M. Masiá, M. Fernández-González, S. Padilla, P. Ortega, J. A. García, V. Agulló, J. García-Abellán, G. Telenti, L. Guillén, F. Gutiérrez, Impact of interleukin-6 blockade with tocilizumab on SARS-CoV-2 viral kinetics and antibody responses in patients with COVID-19: A prospective cohort study. *EBioMedicine* **60**, 102999 (2020).

15. B. Israelow, T. Mao, J. Klein, E. Song, B. Menasche, S. B. Omer, A. Iwasaki, Adaptive immune determinants of viral clearance and protection in mouse models of SARS-CoV-2. *Sci. Immunol.* **6**, eabl4509 (2021).

16. Z. Chen, E. John Wherry, T cell responses in patients with COVID-19. *Nat. Rev. Immunol.* **20**, 529–536 (2020).

17. A. C. Karlsson, M. Humbert, M. Buggert, The known unknowns of T cell immunity to COVID-19. *Sci. Immunol.* **5**, eabe8063 (2020).

18. A. C. Codo, G. G. Davanzo, L. de B. Monteiro, G. F. de Souza, S. P. Muraro, J. V. Virgilio-da-Silva, J. S. Prodonoff, V. C. Carregari, C. A. O. de Biagi Junior, F. Crunfli, J. L. L. Restrepo, P. H. Vendramini, G. Reis-de-Oliveira, K. B. dos Santos, D. A. Toledo-Teixeira, P. L. Parise, M. C. Martini, R. E. Marques, H. R. Carmo, A. Borin, L. D. Coimbra, V. O. Boldrini, N. S. Brunetti, A. S. Vieira, E. Mansour, R. G. Ulaf, A. F. Bernardes, T. A. Nunes, L. C. Ribeiro, A. C. Palma, M. V. Agrela, M. L. Moretti, A. C. Sposito, F. B. Pereira, L. A. Velloso, M. A. R. Vinolo, A. Damasio, J. L. Proença-Módena, R. F. Carvalho, M. A. Mori, D. Martins-de-Souza, H. I. Nakaya, A. S. Farias, P. M. Moraes-Vieira, Elevated glucose levels favor SARS-CoV-2 infection and monocyte response through a HIF-1α/Glycolysis-dependent axis. *Cell Metab.* **32**, 498–499 (2020).

19. M.-S. Rha, H. W. Jeong, J.-H. Ko, S. J. Choi, I.-H. Seo, J. S. Lee, M. Sa, A. R. Kim, E.-J. Joo, J. Y. Ahn, J. H. Kim, K.-H. Song, E. S. Kim, D. H. Oh, M. Y. Ahn, H. K. Choi, J. H. Jeon,

J.-P. Choi, H. B. Kim, Y. K. Kim, S.-H. Park, W. S. Choi, J. Y. Choi, K. R. Peck, E.-C. Shin, PD-1-expressing SARS-CoV-2-specific CD8+ T cells are not exhausted, but functional in patients with COVID-19. *Immunity* **54**, 44–52.e3 (2021).

20. A. J. Wilk, A. Rustagi, N. Q. Zhao, J. Roque, G. J. Martínez-Colón, J. L. McKechnie, G. T. Ivison, T. Ranganath, R. Vergara, T. Hollis, L. J. Simpson, P. Grant, A. Subramanian, A. J. Rogers, C. A. Blish, A single-cell atlas of the peripheral immune response in patients with severe COVID-19. *Nat. Med.* **26**, 1070–1076 (2020).

21. H.-Y. Zheng, M. Zhang, C.-X. Yang, N. Zhang, X.-C. Wang, X.-P. Yang, X.-Q. Dong, Y.-T. Zheng, Elevated exhaustion levels and reduced functional diversity of T cells in peripheral blood may predict severe progression in COVID-19 patients. *Cell. Mol. Immunol.* **17**, 541–543 (2020).

22. M. Zheng, Y. Gao, G. Wang, G. Song, S. Liu, D. Sun, Y. Xu, Z. Tian, Functional exhaustion of antiviral lymphocytes in COVID-19 patients. *Cell. Mol. Immunol.* **17**, 533–535 (2020).

23. R. Zhou, K. K.-W. To, Y.-C. Wong, L. Liu, B. Zhou, X. Li, H. Huang, Y. Mo, T.-Y. Luk, T. T.-K. Lau, P. Yeung, W.-M. Chan, A. K.-L. Wu, K.-C. Lung, O. T.-Y. Tsang, W.-S. Leung, I. F.-N. Hung, K.-Y. Yuen, Z. Chen, Acute SARS-CoV-2 infection impairs dendritic cell and T cell responses. *Immunity* **53**, 864–877.e5 (2020).

24. C. U. Blank, W. N. Haining, W. Held, P. G. Hogan, A. Kallies, E. Lugli, R. C. Lynn, M. Philip, A. Rao, N. P. Restifo, A. Schietinger, T. N. Schumacher, P. L. Schwartzberg, A. H. Sharpe, D. E. Speiser, E. J. Wherry, B. A. Youngblood, D. Zehn, Defining 'T cell exhaustion'. *Nat. Rev. Immunol.* **19**, 665–674 (2019).

25. L. M. McLane, M. S. Abdel-Hakeem, E. J. Wherry, CD8 T cell exhaustion during chronic viral infection and cancer. *Annu. Rev. Immunol.* **37**, 457–495 (2019).

26. D. L. Barber, E. J. Wherry, D. Masopust, B. Zhu, J. P. Allison, A. H. Sharpe, G. J. Freeman, R. Ahmed, Restoring function in exhausted CD8 T cells during chronic viral infection. *Nature* **439**, 682–687 (2006).

27. A. Ribas, J. D. Wolchok, Cancer immunotherapy using checkpoint blockade. *Science* **359**, 1350–1355 (2018).

28. M. Aldea, J.-M. Michot, F.-X. Danlos, A. Ribas, J.-C. Soria, Repurposing of anticancer drugs expands possibilities for antiviral and anti-inflammatory discovery in COVID-19. *Cancer Discov.* **11**, 1336–1344 (2021).

29. M. Hill, M. Segovia, S. Russo, M. Girotti, G. A. Rabinovich, The paradoxical roles of inflammation during PD-1 blockade in cancer. *Trends Immunol.* **41**, 982–993 (2020).

30. F. Martinon, K. Burns, J. Tschopp, The inflammasome. *Mol. Cell* **10**, 417–426 (2002).

31. M. Segovia, S. Russo, M. Jeldres, Y. D. Mahmoud, V. Perez, M. Duhalde, P. Charnet, M. Rousset, S. Victoria, F. Veigas, C. Louvet, B. Vanhove, R. A. Floto, I. Anegon, M. C. Cuturi, M. R. Girotti, G. A. Rabinovich, M. Hill, Targeting TMEM176B enhances antitumor immunity and augments the efficacy of immune checkpoint blockers by unleashing inflammasome activation. *Cancer Cell* **35**, 767–781.e6 (2019).

32. M. Segovia, C. Louvet, P. Charnet, A. Savina, G. Tilly, L. Gautreau, L. Carretero-Iglesia, G. Beriou, I. Cebrian, T. Cens, L. Hepburn, E. Chiffoleau, R. A. Floto, I. Anegon, S. Amigorena, M. Hill, M. C. Cuturi, Autologous dendritic cells prolong allograft survival through *Tmem176b*-dependent antigen cross-presentation. *Am. J. Transplant.* **14**, 1021–1031 (2014).

33. M. Segovia, S. Russo, M. R. Girotti, G. A. Rabinovich, M. Hill, Role of inflammasome activation in tumor immunity triggered by immune checkpoint blockers. *Clin. Exp. Immunol.* **200**, 155–162 (2020).

34. I. Mattiola, A. Mantovani, M. Locati, The tetraspan MS4A family in homeostasis, immunity, and disease. *Trends Immunol.* **42**, 764–781 (2021).

35. K. Pekayvaz, A. Leunig, R. Kaiser, M. Joppich, S. Brambs, A. Janjic, O. Popp, D. Nixdorf, V. Fumagalli, N. Schmidt, V. Polewka, A. Anjum, V. Knottenberg, L. Eivers, L. E. Wange, C. Gold, M. Kirchner, M. Muenchhoff, J. C. Hellmuth, C. Scherer, R. Rubio-Acero, T. Eser, F. Deák, K. Puchinger, N. Kuhl, A. Linder, K. Saar, L. Tomas, C. Schulz, A. Wieser, W. Enard, I. Kroidl, C. Geldmacher, M. von Bergwelt-Baildon, O. T. Keppler, M. Munschauer, M. Iannacone, R. Zimmer, P. Mertins, N. Hubner, M. Hoelscher, K. Stark, L. Nicolai, Protective immune trajectories in early viral containment of non-pneumonic SARS-CoV-2 infection. *Nat. Commun.* **13**, 1018 (2022).

36. M. Liao, Y. Liu, J. Yuan, Y. Wen, G. Xu, J. Zhao, L. Cheng, J. Li, X. Wang, F. Wang, L. Liu, I. Amit, S. Zhang, Z. Zhang, Single-cell landscape of bronchoalveolar immune cells in patients with COVID-19. *Nat. Med.* **26**, 842–844 (2020).

37. M. Zheng, E. P. Williams, R. K. S. Malireddi, R. Karki, B. Banoth, A. Burton, R. Webby, R. Channappanavar, C. B. Jonsson, T.-D. Kanneganti, Impaired NLRP3 inflammasome activation/pyroptosis leads to robust inflammatory cell death via caspase-8/RIPK₃ during coronavirus infection. *J. Biol. Chem.* **295**, 14040–14052 (2020).

38. A. Gupta, M. V. Madhavan, K. Sehgal, N. Nair, S. Mahajan, T. S. Sehrawat, B. Bikdeli, N. Ahluwalia, J. C. Ausiello, E. Y. Wan, D. E. Freedberg, A. J. Kirtane, S. A. Parikh, M. S. Maurer, A. S. Nordvig, D. Accili, J. M. Bathon, S. Mohan, K. A. Bauer, M. B. Leon, H. M. Krumholz, N. Uriel, M. R. Mehra, M. S. V. Elkind, G. W. Stone, A. Schwartz, D. D. Ho, J. P. Bilezikian, D. W. Landry, Extrapulmonary manifestations of COVID-19. *Nat. Med.* **26**, 1017–1032 (2020).

39. S. Guo, C. Yang, B. Diao, X. Huang, M. Jin, L. Chen, W. Yan, Q. Ning, L. Zheng, Y. Wu, Y. Chen, The NLRP3 inflammasome and IL-1β accelerate immunologically mediated pathology in experimental viral fulminant hepatitis. *PLOS Pathog.* **11**, e1005155 (2015).

40. F. Di Pierro, G. Derosa, P. Maffioli, A. Bertuccioli, S. Togni, A. Riva, P. Allegrini, A. Khan, S. Khan, B. A. Khan, N. Altaf, M. Zahid, I. D. Ujjan, R. Nigar, M. I. Khushk, M. Phulpoto, A. Lail, B. R. Devrajani, S. Ahmed, Possible therapeutic effects of adjuvant quercetin supplementation against early-stage COVID-19 infection: A prospective, randomized, controlled, and open-label study. *IJGM* **14**, 2359–2366 (2021).

41. F. Di Pierro, S. Iqtadar, A. Khan, S. Ullah Mumtaz, M. Masud Chaudhry, A. Bertuccioli, G. Derosa, P. Maffioli, S. Togni, A. Riva, P. Allegrini, S. Khan, Potential clinical benefits of quercetin in the early stage of COVID-19: Results of a second, pilot, randomized, controlled and open-label clinical trial. *Int. J. Gen. Med.* **14**, 2807–2816 (2021).

42. F. Alfei, K. Kanev, M. Hofmann, M. Wu, H. E. Ghoneim, P. Roelli, D. T. Utzschneider, M. von Hoesslin, J. G. Cullen, Y. Fan, V. Eisenberg, D. Wohlleber, K. Steiger, D. Merkler, M. Delorenzi, P. A. Knolle, C. J. Cohen, R. Thimme, B. Youngblood, D. Zehn, TOX reinforces the phenotype and longevity of exhausted T cells in chronic viral infection. *Nature* **571**, 265–269 (2019).

43. A. C. Scott, F. Dündar, P. Zumbo, S. S. Chandran, C. A. Klebanoff, M. Shakiba, P. Trivedi, L. Menocal, H. Appleby, S. Camara, D. Zamarin, T. Walther, A. Snyder, M. R. Femia, E. A. Comen, H. Y. Wen, M. D. Hellmann, N. Anandasabapathy, Y. Liu, N. K. Altorki, P. Lauer, O. Levy, M. S. Glickman, J. Kaye, D. Betel, M. Philip, A. Schietinger, TOX is a critical regulator of tumour-specific T cell differentiation. *Nature* **571**, 270–274 (2019).

44. T. Sekine, A. Perez-Potti, S. Nguyen, J.-B. Gorin, V. H. Wu, E. Gostick, S. Llewellyn-Lacey, Q. Hammer, S. Falck-Jones, S. Vangeti, M. Yu, A. Smed-Sörensen, A. Gaballa, M. Uhlin, J. K. Sandberg, C. Brander, P. Nowak, P. A. Goepfert, D. A. Price, M. R. Betts, M. Buggert, TOX is expressed by exhausted and polyfunctional human effector memory CD8+ T cells. *Sci. Immunol.* **5**, eaba7918 (2020).

45. O. Khan, J. R. Giles, S. McDonald, S. Manne, S. F. Ngiow, K. P. Patel, M. T. Werner, A. C. Huang, K. A. Alexander, J. E. Wu, J. Attanasio, P. Yan, S. M. George, B. Bengsch, R. P. Staupe, G. Donahue, W. Xu, R. K. Amaravadi, X. Xu, G. C. Karakousis, T. C. Mitchell, L. M. Schuchter, J. Kaye, S. L. Berger, E. J. Wherry, TOX transcriptionally and epigenetically programs CD8+ T cell exhaustion. *Nature* **571**, 211–218 (2019).

46. M. T. McClain, F. J. Constantine, R. Henao, Y. Liu, E. L. Tsalik, T. W. Burke, J. M. Steinbrink, E. Petzold, B. P. Nicholson, R. Rolfe, B. D. Kraft, M. S. Kelly, D. R. Saban, C. Yu, X. Shen, E. M. Ko, G. D. Sempowski, T. N. Denny, G. S. Ginsburg, C. W. Woods, Dysregulated transcriptional responses to SARS-CoV-2 in the periphery. *Nat. Commun.* **12**, 1079 (2021).

47. T. S. Rodrigues, K. S. Sa, A. Y. Ishimoto, A. Becerra, S. Oliveira, L. Almeida, A. V. Goncalves, D. B. Perucello, W. A. Andrade, R. Castro, F. P. Veras, J. E. Toller-Kawahisa, D. C. Nascimento, M. H. de Lima, C. M. Silva, D. B. Caetite, R. B. Martins, I. A. Castro, M. C. Pontelli, F. C. de Barros, N. B. do Amaral, M. C. Giannini, L. P. Bonjorno, M. I. F. Lopes, M. N. Benatti, R. C. Santana, F. C. Vilar, M. Auxiliadora-Martins, R. Luppino-Assad, S. C. de Almeida, F. R. de Oliveira, S. S. Batah, L. Siyuan, M. N. Benatti, T. M. Cunha, J. C. Alves-Filho, F. Q. Cunha, L. D. Cunha, F. G. Frantz, T. Kohlsdorf, A. T. Fabro, E. Arruda, R. D. de Oliveira, P. Louzada-Junior, D. S. Zamboni, Inflammasome activation in COVID-19 patients. *medRxiv* 2020.08.05.20168872, (2020).

48. G. Cavalli, G. De Luca, C. Campochiaro, E. Della-Torre, M. Ripa, D. Canetti, C. Oltolini, B. Castiglioni, C. T. Din, N. Boffini, A. Tomelleri, N. Farina, A. Ruggeri, P. Rovere-Querini, G. Di Lucca, S. Martinenghi, R. Scotti, M. Tresoldi, F. Ciceri, G. Landoni, A. Zangrillo, P. Scarpellini, L. Dagna, Interleukin-1 blockade with high-dose anakinra in patients with COVID-19, acute respiratory distress syndrome, and hyperinflammation: A retrospective cohort study. *Lancet Rheumatol.* **2**, e325–e331 (2020).

49. T. Huet, H. Beaussier, O. Voisin, S. Jouveshomme, G. Dauriat, I. Lazareth, E. Sacco, J.-M. Naccache, Y. Bézie, S. Laplanche, A. Le Berre, J. Le Pavec, S. Salmeron, J. Emmerich, J.-J. Mourad, G. Chatellier, G. Hayem, Anakinra for severe forms of COVID-19: A cohort study. *Lancet Rheumatol.* **2**, e393–e400 (2020).

50. CORIMUNO-19 Collaborative group, Effect of anakinra versus usual care in adults in hospital with COVID-19 and mild-to-moderate pneumonia (CORIMUNO-ANA-1): A randomised controlled trial. *Lancet Respir. Med.* **9**, 295–304 (2021).

51. E. Y. Wang, T. Mao, J. Klein, Y. Dai, J. D. Huck, J. R. Jaycox, F. Liu, T. Zhou, B. Israelow, P. Wong, A. Coppi, C. Lucas, J. Silva, J. E. Oh, E. Song, E. S. Perotti, N. S. Zheng, S. Fischer, M. Campbell, J. B. Fournier, A. L. Wyllie, C. B. F. Vogels, I. M. Ott, C. C. Kalinich, M. E. Petrone, A. E. Watkins; Yale IMPACT Team, A. Obaid, A. J. Moore, A. Casanovas-Massana, A. Lu-Culligan, A. Nelson, A. Nunez, A. Martin, B. Geng, C. D. Odio, C. A. Harden, C. Todeasa, C. Jensen, D. Kim, D. McDonald, D. Shepard, E. Courchaine, E. B. White, E. Silva, E. Kudo, G. Deluliis, H. Rahming, H.-J. Park, I. Matos, J. Nouws, J. Valdez, J. Lim, K.-A. Rose, K. Anastasio, K. Brower, L. Glick, L. Sharma, L. Sewanan, L. Knaggs, M. Minasyan, M. Batsu, M. Kuang, M. Nakahata, M. Linehan, M. H. Askenase, M. Simonov, M. Smolgovsky, N. Sonnert, N. Naushad, P. Vijayakumar, R. Martinello, R. Datta, R. Handoko, S. Bermejo, S. Prophet, S. Bickerton, S. Velazquez, T. Rice, W. Khoury-Hanold, X. Peng, Y. Yang, Y. Cao, Y. Strong, C. Dela Cruz, S. F. Farhadian, W. L. Schulz, S. Ma, N. D. Grubaugh, A. I. Ko, A. Iwasaki, A. M. Ring, Diverse functional autoantibodies in patients with COVID-19. *Nature* **595**, 283–288 (2021).

52. R.-D. Jiang, M.-Q. Liu, Y. Chen, C. Shan, Y.-W. Zhou, X.-R. Shen, Q. Li, L. Zhang, Y. Zhu, H.-R. Si, Q. Wang, J. Min, X. Wang, W. Zhang, B. Li, H.-J. Zhang, R. S. Baric, P. Zhou,

X.-L. Yang, Z.-L. Shi, Pathogenesis of SARS-CoV-2 in transgenic mice expressing human angiotensin-converting enzyme 2. *Cell* **182**, 50–58.e8 (2020).

53. K. Chang, C. Svabek, C. Vazquez-Guillamet, B. Sato, D. Rasche, S. Wilson, P. Robbins, N. Ulbrandt, J. Suzich, J. Green, A. C. Patera, W. Blair, S. Krishnan, R. Hotchkiss, Targeting the programmed cell death 1: Programmed cell death ligand 1 pathway reverses T cell exhaustion in patients with sepsis. *Crit. Care* **18**, R3 (2014).

54. Y. Nakamori, E. J. Park, M. Shimaoka, Immune deregulation in sepsis and septic shock: Reversing immune paralysis by targeting PD-1/PD-L1 pathway. *Front. Immunol.* **11**, 624279 (2021).

55. D. Guinault, M.-L. Nicolau-Travers, S. Silva, O. Cointault, B. Daniau, A. Del Bello, M. Peres, D. Rousset, J. Rieunier, L. Lavayssiere, M.-B. Nogier, E. Hourcastagnou, A. Mari, N. Kamar, F. Vergez, S. Faguer, Expression of exhaustion markers on CD8+ T-cell patterns predict outcomes in septic patients admitted to the ICU*. *Crit. Care Med.* **49**, 1513–1523 (2021).

56. N. Yatim, J. Boussier, P. Tetu, N. Smith, T. Bruel, B. Charbit, L. Barnabei, A. Corneau, L. Da Meda, C. Allayous, B. Baroudjian, M. Jebali, F. Herms, L. Grzelak, I. Staropoli, V. Calmettes, J. Hadjadj, O. Peyrony, C. Cassius, J. LeGoff, N. Kramkimel, S. Aractingi, M. Fontes, C. Blanc, F. Rieux-Laucat, O. Schwartz, B. Terrier, D. Duffy, C. Lebbé, Immune checkpoint inhibitors increase T cell immunity during SARS-CoV-2 infection. *Sci. Adv.* **7**, eabg4081 (2021).

57. L. Albiges, S. Foulon, A. Bayle, B. Gachot, F. Pommeret, C. Willekens, A. Stoclin, M. Merad, F. Griscelli, L. Lacroix, F. Netzer, T. Hueso, C. Balleyguier, S. Ammari, E. Colomba, G. Baciarello, A. Perret, A. Hollebecque, J. Hadoux, J.-M. Michot, N. Chaput, V. Saada, M. Hauchecorne, J.-B. Micol, R. Sun, D. Valteau-Couanet, F. André, F. Scotte, B. Besse, J.-C. Soria, F. Barlesi, Determinants of the outcomes of patients with cancer infected with SARS-CoV-2: Results from the Gustave Roussy cohort. *Nat. Cancer* **1**, 965–975 (2020).

58. E. V. Robilotti, N. E. Babady, P. A. Mead, T. Rolling, R. Perez-Johnston, M. Bernardes, Y. Bogler, M. Caldararo, C. J. Figueroa, M. S. Glickman, A. Joanow, A. Kaltsas, Y. J. Lee, A. Lucca, A. Mariano, S. Morjaria, T. Nawar, G. A. Papanicolaou, J. Predmore, G. Redelman-Sidi, E. Schmidt, S. K. Seo, K. Sepkowitz, M. K. Shah, J. D. Wolchok, T. M. Hohl, Y. Taur, M. Kamboj, Determinants of COVID-19 disease severity in patients with cancer. *Nat. Med.* **26**, 1218–1223 (2020).

59. R. S. Hotchkiss, E. Colston, S. Yende, E. D. Crouser, G. S. Martin, T. Albertson, R. R. Bartz, S. C. Brakenridge, M. J. Delano, P. K. Park, M. W. Donnino, M. Tidswell, F. B. Mayr, D. C. Angus, C. M. Coopersmith, L. L. Moldawer, I. M. Catlett, I. G. Girgis, J. Ye, D. M. Grasela, Immune checkpoint inhibition in sepsis: A phase 1b randomized study to evaluate the safety, tolerability, pharmacokinetics, and pharmacodynamics of nivolumab. *Intensive Care Med.* **45**, 1360–1371 (2019).

60. J. C. Marshall, S. Murthy, J. Diaz, N. K. Adhikari, D. C. Angus, Y. M. Arabi, K. Baillie, M. Bauer, S. Berry, B. Blackwood, M. Bonten, F. Bozza, F. Brunkhorst, A. Cheng, M. Clarke, V. Q. Dat, M. de Jong, J. Denholm, L. Derde, J. Dunning, X. Feng, T. Fletcher, N. Foster, R. Fowler, N. Gobat, C. Gomersall, A. Gordon, T. Glueck, M. Harhay, C. Hodgson, P. Horby, Y. Kim, R. Kojan, B. Kumar, J. Laffey, D. Malvey, I. Martin-Loeches, C. McArthur, D. McAuley, S. McBride, S. McGuinness, L. Merson, S. Morpeth, D. Needham, M. Netea, M.-D. Oh, S. Phyu, S. Piva, R. Qiu, H. Salisu-Kabara, L. Shi, N. Shimizu, J. Sinclair, S. Tong, A. Turgeon, T. Uyeki, F. van de Veerdonk, S. Webb, P. Williamson, T. Wolf, J. Zhang, A minimal common outcome measure set for COVID-19 clinical research. *Lancet Infect. Dis.* **20**, e192–e197 (2020).